Interplane charge dynamics in a valence-bond dynamical mean-field theory of cuprate superconductors

M. Ferrero,[1] O. Parcollet,[2] A. Georges,[1,3] G. Kotliar,[4] and D. N. Basov[5]

[1]*Centre de Physique Théorique, Ecole Polytechnique, CNRS, 91128 Palaiseau Cedex, France*
[2]*Institut de Physique Théorique (IPhT), CEA, CNRS, URA 2306, 91191 Gif-sur-Yvette, France*
[3]*Collège de France, 11 place Marcelin Berthelot, 75005 Paris, France*
[4]*Physics Department and Center for Materials Theory, Rutgers University, Piscataway, New Jersey 08854, USA*
[5]*Department of Physics, University of California–San Diego, La Jolla, California 92093, USA*

We present calculations of the interplane charge dynamics in the normal state of cuprate superconductors within the valence-bond dynamical mean-field theory. We show that by varying the hole doping, the *c*-axis optical conductivity and resistivity dramatically change character, going from metalliclike at large doping to insulatinglike at low doping. We establish a clear connection between the behavior of the *c*-axis optical and transport properties and the destruction of coherent quasiparticles as the pseudogap opens in the antinodal region of the Brillouin zone at low doping. We show that our results are in good agreement with spectroscopic and optical experiments.

I. INTRODUCTION

Even after many years of investigation, cuprate superconductors continue to be at the center of intense experimental and theoretical interest. A key phenomenon which needs to be understood to reveal the nature of superconductivity in the cuprates is the onset of strong momentum-space differentiation in the (hole-) underdoped normal state. This region of the phase diagram is characterized by the suppression of quasiparticle excitations in the antinodal region of the Brillouin zone and the opening of a pseudogap yielding Fermi arcs, as observed, e.g., in angle-resolved photoemission (ARPES) experiments.[1] Other distinctive properties of the cuprates are seen in the extreme anisotropy of the charge dynamics.[2–5] The in-plane (ρ_{ab}) and interplane resistivities (ρ_c) have different temperature dependence. While ρ_{ab} decreases with decreasing temperatures at all doping levels, ρ_c is sensitive to the doping. Its behavior is essentially insulating at low doping, semimetallic at intermediate doping, and metallic in the overdoped regime. The peculiar properties of the interplane charge dynamics have also been observed in optical studies.[5–13] They reveal that the *c*-axis optical conductivity $\sigma_c(\Omega)$ shows no sharp Drude peak at low frequencies Ω in the underdoped normal state. Instead, $\sigma_c(\Omega)$ has a rather flat frequency dependence at temperatures above the pseudogap temperature T^*. As the temperature is reduced below T^*, low-energy spectral weight is transferred to higher energies and $\sigma_c(\Omega)$ displays a gaplike depression as $\Omega \rightarrow 0$. Only in the highly overdoped region does $\sigma_c(\Omega)$ show evidence of emerging coherence.[8]

In this paper, we address the interplane charge dynamics of cuprate superconductors within the valence-bond dynamical mean-field theory (VB-DMFT) introduced in Refs. 14 and 15. Our results capture many salient features found in experiments for the *c*-axis resistivity and optical conductivity. Specifically, we show that the opening of a pseudogap in the antinodal region explains the incoherent behavior of the interplane transport.

The VB-DMFT is a minimal cluster extension of the dynamical mean-field theory[16,17] that aims at describing momentum-space differentiation together with Mott physics. We apply it to the Hubbard model on a square lattice defined by the Hamiltonian

$$\mathcal{H} = \sum_{\mathbf{k},\sigma} \epsilon_{\mathbf{k}} c^{\dagger}_{\sigma,\mathbf{k}} c_{\sigma,\mathbf{k}} + U \sum_i n_{i\uparrow} n_{i\downarrow},$$

$$\epsilon_{\mathbf{k}} = -2t[\cos(\mathbf{k}_x) + \cos(\mathbf{k}_y)] - 4t' \cos(\mathbf{k}_x)\cos(\mathbf{k}_y), \quad (1)$$

where t and t' are the nearest- and next-nearest-neighbor hopping and U is the on-site Coulomb repulsion. In the following, we use $U/t=10$ and $t'/t=-0.3$, which are values commonly used for modeling hole-doped cuprates in a single-band framework. This value of U is larger than the critical value for the Mott transition in the undoped model so that we deal with a doped Mott insulator. VB-DMFT is based on an effective two-impurity model embedded in a self-consistent bath. Within this simple approach involving only two degrees of freedom, the lattice self-energy is approximated to be piecewise constant over two patches of the Brillouin zone. These two patches are shown in Fig. 1. Inspired by the phenomenology of cuprate superconductors, their shape is chosen in such a way that the central (red) patch covers the nodal region of the Fermi surface while the border (blue) patch covers the antinodal region. With this prescription, one degree of freedom of the underlying two-impurity model is associated with the physics of nodal quasiparticles and the other degree of freedom with antinodal quasiparticles. Thanks to the relative simplicity of the VB-DMFT approach, it is possible to make very efficient calculations using continuous-time quantum Monte Carlo and obtain accurate spectral functions $A(\mathbf{k},\omega)$. More details concerning this procedure are given in Appendix and in Refs. 14 and 15.

In the VB-DMFT, the formation of Fermi arcs is described by a selective metal-insulator transition in momentum space.[14,15] Below a doping ~16%, the degree of free-

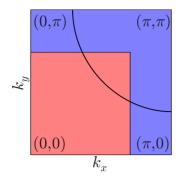FIG. 1. (Color online) The two patches dividing the Brillouin zone. The line shows a noninteracting Fermi surface for the dispersion $\epsilon_{\mathbf{k}}$ of Eq. (1). The central (red) patch covers the nodal region of the Fermi surface while the border (blue) patch covers the antinodal region.

dom describing the antinodal regions becomes insulating while that associated to the nodal quasiparticles remains metallic. The orbital-selective mechanism responsible for the pseudogap has also been confirmed in studies involving larger clusters.[18–20] In Refs. [14] and [15], we used the VB-DMFT to compute tunneling and ARPES spectra in good agreement with experiments.

II. INTERPLANE OPTICAL CONDUCTIVITY

We first compute the frequency-dependent c-axis optical conductivity $\sigma_c(\Omega)$, given by

$$\sigma_c(\Omega) = \frac{2e^2c}{\hbar ab} \int d\omega \frac{f(\omega) - f(\omega + \Omega)}{\Omega} \frac{1}{N} \sum_{\mathbf{k}} t_\perp^2(\mathbf{k}) A(\mathbf{k}, \omega) A(\mathbf{k}, \Omega + \omega),$$

$$\tag{2}$$

where f is the Fermi function, $A(\mathbf{k}, \omega)$ the in-plane spectral

function, N the number of lattice sites, e the electronic charge, a, b the in-plane lattice constants, c the interplane distance, and $t_\perp(\mathbf{k}) = t_0[\cos(\mathbf{k}_x) - \cos(\mathbf{k}_y)]^2$ the interplane tunneling matrix element.[21,22] Note that in this expression $t_\perp(\mathbf{k})$ has a strong $\mathbf{k}$ dependence with contributions stemming mainly from the antinodal region of the Brillouin zone. For convenience, we will express energies in units of the half-bandwidth D of the electronic dispersion and the optical conductivity in units of $\sigma^* = 2e^2 c t_0^2 / \hbar ab D^2$. In YBa$_2Cu_3O_y$ compounds, $D \sim 1$ eV ~ 8000 cm^{-1} and σ^* is of order $\sigma^* \sim 50$ Ω^{-1} cm^{-1}.

In the left panel of Fig. 2, we display the computed $\sigma_c(\Omega)$ for three levels of hole doping and several temperatures. Our results show three distinctive behaviors. At high doping $\delta \gtrsim 16\%$, the conductivity displays a metalliclike behavior with the buildup of a Drude-type peak as the temperature is decreased. Note that as the peak increases additional spectral weight appears at low energy. At low doping $\delta \lesssim 10\%$, $\sigma_c(\Omega)$ is characterized by a gaplike depression at low frequencies where spectral weight is suppressed with decreasing temperature. The width of the gap when it opens at high temperature is $\sim 0.15D$ and remains approximately the same as the temperature is lowered. Note that the spectral weight that is lost in the gap is redistributed over a wide range of energies. The appearance of the depression in the spectra can be directly linked to the formation of a pseudogap in the antinodal region.[14,15] Indeed, the matrix element $t_\perp$ appearing in the expression of the optical conductivity Eq. (2) essentially probes the region[25] close to $(\pm\pi, 0)$, $(0, \pm\pi)$ so that a loss of coherent antinodal quasiparticles results in a loss of low-energy spectral weight in the c-axis optical conductivity. In Refs. [14] and [15], it has been shown that in a zero-temperature analysis of VB-DMFT, coherent quasiparticles disappear in the antinodal region at a doping $\sim 16\%$. This is consistent with σ_c showing a depression only for doping levels below
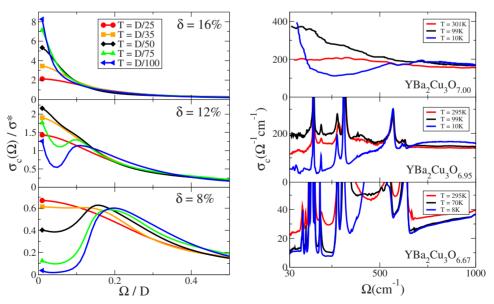

FIG. 2. (Color online) Left panel: the c-axis optical conductivity $\sigma_c(\Omega)$ calculated within VB-DMFT for three doping levels. σ_c is displayed in units of σ^* as defined in the text (σ^* is of order 50 Ω^{-1} cm^{-1} for YBa$_2$Cu$_3$O$_y$). Frequency is normalized to the half-bandwidth $D \sim 1$ eV$= 8000$ cm^{-1}. Right panel: experimental data for the c-axis optical conductivity of YBa$_2$Cu$_3$O$_y$. The data for YBa$_2$Cu$_3$O$_{7.00}$ is taken from Ref. [8] where the phonon contribution was subtracted by fitting to five Lorentzian oscillators. The data for YBa$_2$Cu$_3$O$_{6.95}$ and YBa$_2$Cu$_3$O$_{6.67}$ are taken from Refs. [23] and [24].
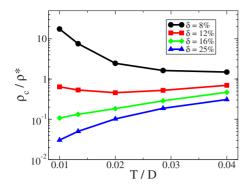
FIG. 3. (Color online) The c-axis resistivity ρ_c calculated within the VB-DMFT for four doping levels as a function of temperature.

~16%. At intermediate doping, $\sigma_c(\Omega)$ has a mixed character (see left panel of Fig. 2 for $\delta=12\%$). Starting from high temperatures, the low-energy conductivity first displays metallic behavior with an increase in σ_c as the temperature is lowered. At temperatures $T < D/50$, however, a gap starts to appear and low-energy spectral weight is suppressed.

The right panel of Fig. 2 displays the experimental interplane optical conductivity of $YBa_2Cu_3O_y$ obtained in Refs. 8, 23, and 24. At large doping levels, the data show a buildup of a Drude peak consistent with our theoretical calculation. One must note, however, that the interplane optical conductivity of $YBa_2Cu_3O_7$ displays a crossing between the spectra at different temperatures and that the spectral weight transfer is not as clear as in the theoretical curves (left panel) for $\delta=16\%$. In fact, only at doping levels larger than $\delta \sim 25\%$ do the computed σ_c eventually behave more metalliclike with a sharp Drude peak at low energies. This behavior is also consistent with other experiments, e.g., on overdoped $YBa_2Cu_3O_y$, see Fig. 1 of Ref. 26. At low doping, the spectra of $YBa_2Cu_3O_{6.67}$ display the opening of a gaplike depression, which is quite well captured by our theoretical results. Remarkably, σ_c is typically a factor of ten smaller than that in $YBa_2Cu_3O_7$, a factor quantitatively similar to what we obtain theoretically by comparing our results for $\delta=16\%$ and $\delta=8\%$. At intermediate doping between these two limits, $YBa_2Cu_3O_{6.95}$ displays spectra which depend on temperature in a nonmonotonous manner, first increasing upon cooling and then decreasing at lower temperatures. This behavior is indeed observed in our theoretical results at 12% doping. All these observations show that our calculations agree qualitatively, and to a certain extent quantitatively, with optical conductivity measurements on underdoped cuprates (see also, e.g., Ref. 5, Fig. 2 in Ref. 7 or Fig. 1 in Ref. 27).

III. INTERPLANE RESISTIVITY

From the $\Omega=0$ extrapolation of the optical conductivity, we obtain the c-axis resistivity $\rho_c=1/\sigma_c(\Omega=0)$ displayed in Fig. 3 for different doping levels, as a function of temperature. ρ_c is displayed in units of $\rho^*=1/\sigma^*$ which takes the value ~0.02 Ω cm in $YBa_2Cu_3O_y$. As already discussed for the optical conductivity, the properties of ρ_c strongly depend on the doping level. At low doping ($\delta=8\%$), $\rho_c(T)$ has an insulating behavior with a large increase as the temperature

is lowered. This increase is a direct consequence of the opening of the pseudogap in the antinodal region of the Brillouin zone.

As the doping level is increased (see $\delta=12\%$), $\rho_c(T)$ starts to display a mixed, nonmonotonous behavior: it has a minimum as it changes from metalliclike to insulatinglike as T decreases. This behavior is indeed observed in interplane resistivity measurements on $La_{2-x}Sr_xCuO_4$ (Fig. 3 in Ref. 2, Fig. 2 in Ref. 3), $YBa_2Cu_3O_y$ (Fig. 1 in Ref. 4), or $Bi_2Sr_2CaCu_2O_y$ thin films (inset of Fig. 3 in Ref. 28). As we go to higher doping, $\rho_c(T)$ eventually acquires a metalliclike behavior with $d\rho_c/dT>0$. Note that this metallic behavior emerges from the transfer of spectral weight to lower energies as can be seen from Fig. 2. Moreover, even at the largest doping level $\delta=25\%$, $\rho_c(T)$ does not recover the standard Fermi-liquid behavior with $\rho_c(T) \sim T^2$ [closer inspection instead shows that $\rho_c(T)$ roughly behaves as T^α with $\alpha \approx 1.6$]. One might need to consider even larger doping levels to recover a T^2 behavior as seen, e.g., in heavily doped $La_{2-x}Sr_xCuO_4$.[2]

IV. CONCLUSIONS

To conclude, in this paper we have computed the interplane charge dynamics within the VB-DMFT framework in order to address the properties of the normal state of high-T_c copper-oxide superconductors. Our results show that the interplane charge dynamics of the normal state is characterized by three regimes. (i) An overdoped regime where both the c-axis optical conductivity and resistivity show a metalliclike behavior. (ii) An underdoped regime where the destruction of coherent quasiparticles in the antinodal region induces a gaplike depression in σ_c and a resulting insulatinglike interlayer resistivity which increases as temperature is lowered. (iii) An intermediate-doping-mixed regime with first the buildup of a coherence peak in σ_c as the temperature is decreased, followed by a loss of low-energy spectral weight as the pseudogap opens at lower temperatures. As a consequence, ρ_c has a nonmonotonic behavior with a minimum at intermediate temperature. Our calculations are in good agreement with spectroscopic and transport experiments.

Note added. After initial submission of this manuscript, Lin, Gull, and Millis (arXiv:1004.2999) reported calculations of c-axis optical conductivity in eight-site cluster DMFT. When comparison is possible, consistency between these results and our VB-DMFT (two site) results is observed.

APPENDIX: DETAILS ABOUT THE VB-DMFT APPROACH

Let us give here some technical details and briefly describe how our results were obtained. Within the VB-DMFT, the effective model that one has to solve is a two-impurity Anderson model.[14,15] The even (+) combination of the two impurity orbitals is associated with the nodal part of the Brillouin zone while the odd (−) combination is associated to the antinode. The Anderson impurity model is solved using a continuous-time quantum Monte Carlo algorithm[29,30] that yields the even (respectively, odd) orbital self-energy $\Sigma_+(i\omega_n)$ [respectively, $\Sigma_-(i\omega_n)$] at the Matsubara frequencies $i\omega_n$. At this stage one can readily get the quasiparticle residues by carefully extrapolating $\Sigma_{\pm}(i\omega_n)$ at zero frequency

$$Z_{\pm} = \left(1 - \frac{d\,\mathrm{Im}\,\Sigma_{\pm}(i\omega_n)}{d\omega_n}\bigg|_{\omega_n \to 0}\right)^{-1}. \qquad (A1)$$

The inverse quasiparticle lifetime is then given by

$$\Gamma_{\pm} = -Z_{\pm}\,\mathrm{Im}\,\Sigma_{\pm}(i\omega_n)\big|_{\omega_n \to 0}. \qquad (A2)$$

Finally, the nodal (Γ_N) and antinodal (Γ_{AN}) inverse lifetimes are associated with Γ_+ and Γ_-, respectively. In order to compute the optical conductivity and the resistivities it is necessary to have access to the in-plane spectral function $A(\mathbf{k},\omega)$. A first step is to analytically continue the self-energies $\Sigma_{\pm}$ on the real-frequency axis, which is achieved using Padé approximants.[31] This is made possible thank to the extremely accurate, low-noise imaginary-time data. A second step is to interpolate the self-energy to obtain a $\mathbf{k}$-dependent $\Sigma(\mathbf{k},\omega)$ from which the spectral function will be computed. References[14,15] have shown that an efficient interpolation procedure is the M interpolation.[32,33] The self-energy is obtained with $\Sigma(\mathbf{k},\omega) = \omega + \mu - M(\mathbf{k},\omega)^{-1}$, where the cumulant $M(\mathbf{k},\omega)$ is given by

$$M(\mathbf{k},\omega) = \frac{\alpha_+(\mathbf{k})}{\omega + \mu - \Sigma_+(\omega)} + \frac{\alpha_-(\mathbf{k})}{\omega + \mu - \Sigma_-(\omega)} \qquad (A3)$$

with $\alpha_{\pm}(\mathbf{k}) = \frac{1}{2}\{1 \pm \frac{1}{2}[\cos(\mathbf{k}_x) + \cos(\mathbf{k}_y)]\}$. Finally, the spectral function is computed with

$$A(\mathbf{k},\omega) = \frac{1}{\omega + \mu - \epsilon_{\mathbf{k}} - \Sigma(\mathbf{k},\omega)}, \qquad (A4)$$

where $\epsilon_{\mathbf{k}}$ is the square lattice dispersion.

[1] A. Damascelli, Z. Hussain, and Z.-X. Shen, Rev. Mod. Phys. **75**, 473 (2003).

[2] T. Ito, H. Takagi, S. Ishibashi, T. Ido, and S. Uchida, Nature (London) **350**, 596 (1991).

[3] Y. Nakamura and S. Uchida, Phys. Rev. B **47**, 8369 (1993).

[4] K. Takenaka, K. Mizuhashi, H. Takagi, and S. Uchida, Phys. Rev. B **50**, 6534 (1994).

[5] D. N. Basov and T. Timusk, Rev. Mod. Phys. **77**, 721 (2005).

[6] S. L. Cooper *et al.*, Phys. Rev. B **47**, 8233 (1993).

[7] C. C. Homes, T. Timusk, R. Liang, D. A. Bonn, and W. N. Hardy, Phys. Rev. Lett. **71**, 1645 (1993).

[8] J. Schützmann, S. Tajima, S. Miyamoto, and S. Tanaka, Phys. Rev. Lett. **73**, 174 (1994).

[9] K. Tamasaku, Y. Nakamura, and S. Uchida, Phys. Rev. Lett. **69**, 1455 (1992).

[10] K. Tamasaku, T. Ito, H. Takagi, and S. Uchida, Phys. Rev. Lett. **72**, 3088 (1994).

[11] A. V. Puchkov, D. N. Basov, and T. Timusk, J. Phys.: Condens. Matter **8**, 10049 (1996).

[12] D. N. Basov, R. Liang, B. Dabrowski, D. A. Bonn, W. N. Hardy, and T. Timusk, Phys. Rev. Lett. **77**, 4090 (1996).

[13] A. V. Puchkov, P. Fournier, D. N. Basov, T. Timusk, A. Kapitulnik, and N. N. Kolesnikov, Phys. Rev. Lett. **77**, 3212 (1996).

[14] M. Ferrero, P. S. Cornaglia, L. D. Leo, O. Parcollet, G. Kotliar, and A. Georges, EPL **85**, 57009 (2009).

[15] M. Ferrero, P. S. Cornaglia, L. De Leo, O. Parcollet, G. Kotliar, and A. Georges, Phys. Rev. B **80**, 064501 (2009).

[16] A. Georges, G. Kotliar, W. Krauth, and M. J. Rozenberg, Rev. Mod. Phys. **68**, 13 (1996).

[17] T. Maier, M. Jarrell, T. Pruschke, and M. H. Hettler, Rev. Mod. Phys. **77**, 1027 (2005).

[18] E. Gull, O. Parcollet, P. Werner, and A. J. Millis, Phys. Rev. B **80**, 245102 (2009).

[19] P. Werner, E. Gull, O. Parcollet, and A. J. Millis, Phys. Rev. B **80**, 045120 (2009).

[20] E. Gull, M. Ferrero, O. Parcollet, A. Georges, and A. Millis, arXiv:1007.2592 (unpublished).

[21] O. K. Andersen, A. I. Liechtenstein, O. Jepsen, and F. Paulsen, J. Phys. Chem. Solids **56**, 1573 (1995).

[22] L. B. Ioffe and A. J. Millis, Phys. Rev. B **58**, 11631 (1998).

[23] A. D. LaForge, W. J. Padilla, K. S. Burch, Z. Q. Li, A. A. Schafgans, K. Segawa, Y. Ando, and D. N. Basov, Phys. Rev. Lett. **101**, 097008 (2008).

[24] A. D. LaForge, W. J. Padilla, K. S. Burch, Z. Q. Li, A. A. Schafgans, K. Segawa, Y. Ando, and D. N. Basov, Phys. Rev. B **79**, 104516 (2009).

[25] S. Chakravarty, A. Sudbø, P. W. Anderson, and S. Strong, Science **261**, 337 (1993).

[26] J. Schützmann, S. Tajima, S. Miyamoto, and S. Tanaka, J. Phys. Chem. Solids **56**, 1839 (1995).

[27] C. C. Homes, S. V. Dordevic, D. A. Bonn, R. Liang, W. N. Hardy, and T. Timusk, Phys. Rev. B **71**, 184515 (2005).

[28] H. Raffy, V. Toma, C. Murrills, and Z. Z. Li, Physica C **460-462**, 851 (2007).

[29] P. Werner, A. Comanac, L. de' Medici, M. Troyer, and A. J. Millis, Phys. Rev. Lett. **97**, 076405 (2006).

[30] P. Werner and A. J. Millis, Phys. Rev. B **74**, 155107 (2006).

[31] H. J. Vidberg and J. W. Serene, J. Low Temp. Phys. **29**, 179 (1977).

[32] T. D. Stanescu and G. Kotliar, Phys. Rev. B **74**, 125110 (2006).

[33] T. D. Stanescu, M. Civelli, K. Haule, and G. Kotliar, Ann. Phys. **321**, 1682 (2006).